Recursive ESPRIT Algorithm for Multi-User OAM Low-Overhead AoA Estimation

Wen-Xuan Long, *Graduate Student Member, IEEE,* Rui Chen, *Member, IEEE* and Marco Moretti, *Member, IEEE*

***Abstract*—Multi-user orbital angular momentum (MU-OAM) wireless backhaul systems require precise alignment of transmitted and received OAM beams. Therefore, a crucial feature for a macro base station (MBS) is to accurately obtain the angle of arrival (AoA) of OAM beams from the small base stations (SBSs) in the system. Considering the limitations of existing OAM-based AoA estimations, we propose a novel super-resolution AoA estimation method, denoted as the *recursive estimation of signal parameters via rotational invariance techniques (ESPRIT)* method. The proposed technique is fundamentally different from traditional ESPRIT algorithm: It is not based on the displacement-invariant array structure, but on the recursive characteristic of Bessel functions in OAM signals. With this method, the inter-mode interference of the MU-OAM system can be significantly suppressed by less training overhead, and the performance is close to that of the ideal system.**

***Index Terms*—Orbital angular momentum (OAM), wireless backhaul, angle of arrival (AoA) estimation, estimation of signal parameters via rotational invariance techniques (ESPRIT) algorithm.**

I. Introduction

Novel service requirements fuel the need for developing wireless communication networks. The rapid rise of novel applications, e.g., virtual reality, digital twin, auto-pilot driving and holographic video, lead to a surge in mobile data traffic, such that the capacity of next-generation 6G wireless communication networks will reach 100 times that of existing 5G networks [1], [2]. To match the growing demand, more and more high-frequency bands, e.g., terahertz (0.1-10 THz) and millimeter-wave (30-300 GHz) bands, are being licensed [3]. Due to the shortage of radio frequency (RF) spectrum resources, in addition to making available more frequency bandwidth, advanced frequency multiplexing technologies are increasingly crucial. Heterogeneous networks (HetNets), which combine flexible backhaul connections, multiple-input multiple-output (MIMO) and distributed caching technologies [4]–[6], are an essential component of future 6G wireless communication networks. As shown in Fig.1, HetNet typically consists of two types of base stations: a macro base station (MBS) and multiple small base stations (SBSs). The backhaul links between the MBS tier and SBS tier can utilize wireless and/or wired connectivity. In next-generation 6G networks, considering the deployment cost and the massive number of small cells, wireless backhaul [7], [8] will become an efficient solution for handling the backhaul connectivity of numerous small cells.

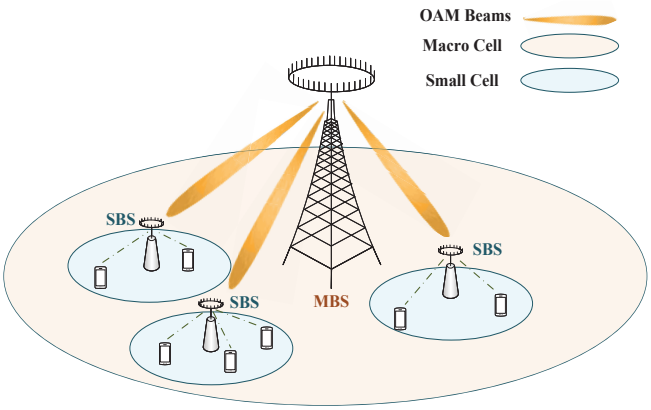

Fig. 1: The application of MU-OAM technology in the PtMP wireless backhaul scenario [9].

High-capacity point-to-multipoint (PtMP) backhauling can be achieved by employing multi-user orbital angular momentum (MU-OAM) technology [9]. The phase front of a vortex electromagnetic (EM) wave with OAM is not planar, but rotates around the transmission axis, revealing a helical structure $e^{i\ell\phi'}$ in space, where ℓ is an integer *OAM mode number* [10] and ϕ' is the transverse azimuth. Benefitting from the space division and the intrinsic orthogonality among different modes, MU-OAM enables different users to multiplex the same set of OAM modes on the same frequency channel simultaneously, thus achieving high spectral efficiency (SE) [9], [11]–[15]. Nevertheless, there are still a number of technical obstacles in the way of the commercial deployment of MU-OAM wireless backhauling.

A special challenge is that OAM requires precise alignment of the transmitted and received beams [9], [13], [16], [17]. If such a condition is not accurately met, the system performance deteriorates significantly. Thus, in MU-OAM systems, reliable angle of arrival (AoA) estimation is indispensable for the MBS. Up to now, the planar wave-based AoA estimation has been widely studied [18]–[20], but AoA estimation for OAM beams remains an open problem and, to these authors' knowledge, [9] is the *only research* focused on the MU-OAM AoA estimation. However, [9] applies the fast Fourier transforms (FFT) method to estimate AoA of OAM beams, which consumes a large number of samples in the OAM mode and frequency domains to meet the required estimation accuracy.

Considering the limitations of existing OAM-based AoA

Wen-Xuan Long is with the School of Telecommunication Engineering, Xidian University, China, and also with the Department of Information Engineering, University of Pisa, Italy (e-mail: wxlong@stu.xidian.edu.cn).

R. Chen is with the State Key Laboratory of Integrated Service Networks (ISN), Xidian University, Shaanxi 710071, China, and also with the National Mobile Communications Research Laboratory, Southeast University, Nanjing 210018, China (e-mail: rchen@xidian.edu.cn).

Marco Moretti is with the Department of Information Engineering, University of Pisa, Italy (e-mail: marco.moretti@unipi.it).

estimation methods, we propose a novel super-resolution AoA estimation method, whose overall steps are similar to the estimation of signal parameters via rotational invariance techniques (ESPRIT) algorithm [21]. However, the proposed method is fundamentally different from the traditional ESPRIT algorithm. It is not based on the displacement-invariant array structure required by the ESPRIT algorithm, but on the recursive characteristic of the Bessel functions in OAM signals, thus being denoted as the recursive ESPRIT algorithm. Compared to the existing FFT-based estimation method [9], the proposed recursive ESPRIT algorithm can directly obtain the closed-form solution of azimuth and elevation angles only by signal processing in the OAM mode domain, thus

- significantly saving the training overhead in the frequency domain,
- significantly improving the estimation accuracy under medium and high signal-to-noise ratio (SNR).

Finally, the MU-OAM system can achieve higher SE due to more payload and lower inter-mode interference. Simulation results show that the proposed algorithm indeed outperforms [9] with less training overhead.

II. UCA-based Multi-User OAM Wireless Backhaul System

Considering the necessity of using uniform circular arrays (UCA) to generate and receive radio OAM beams [22], [23], we propose a UCA-based MU-OAM wireless backhaul system, as shown in Fig.2, which consists of one MBS with an N-element UCA and Q SBSs with M-element UCA. The UCAs of MBS and the Q SBSs are off-axis misaligned [24]. Specifically, the UCA centers of Q SBSs are not coaxial, and the UCA plans of MBS and Q SBSs are parallel. In the geometrical model shown in Fig.2, the coordinate system $\mathrm{Z}_M-\mathrm{X}_M\mathrm{O}_M\mathrm{Y}_M$ is set at MBS taking the UCA plane as the $\mathrm{X}_M\mathrm{O}_M\mathrm{Y}_M$ plane and the axis perpendicular to the UCA plane and passing through the point O_M as the Z_M-axis, and the coordinate systems $\{\mathrm{Z}_q^S-\mathrm{X}_q^S\mathrm{O}_q^S\mathrm{Y}_q^S|q=1,2,\cdots,Q\}$ are set at Q SBSs respectively in a similar manner. The UCA center coordinate of the q-th SBS is defined as $\mathrm{O}_q^S(r_q,\theta_q,\varphi_q)$ in $\mathrm{Z}_M-\mathrm{X}_M\mathrm{O}_M\mathrm{Y}_M$. Then, based on the geometric relationship, the UCA center coordinate of MBS can be written as $\mathrm{O}_M(r_q,\theta_q,\varphi_q+\pi)$ in $\mathrm{Z}_q^S-\mathrm{X}_q^S\mathrm{O}_q^S\mathrm{Y}_q^S$, where r_q is the distance of the UCA centers between MBS and the q-th SBS, θ_q $(0\le\theta_q\le\pi/2)$ and φ_q $(0\le\varphi_q\le2\pi)$ are the elevation angle and the azimuth angle of the q-th SBS UCA center in $\mathrm{Z}_M-\mathrm{X}_M\mathrm{O}_M\mathrm{Y}_M$, and (θ_q,φ_q) *is defined as AoA of OAM beams from the q-th SBS,* $q=1,2,\cdots,Q$.

To realize precise alignment of the transmitted and received OAM beams, the MBS is required to accurately estimate the AoAs of the Q SBSs in the training phase [9], [13], [25]. To do so, the MBS first broadcasts a message to the Q SBSs to start training. After receiving this signal, all the Q SBSs simultaneously transmit their training signals to the MBS, multiplexed on $2P+1$ ($P>Q$, $-\ell_P\le\ell_{\bar{p}}\le\ell_P$, $0\le\ell_P<\lfloor M/2\rfloor$) OAM modes, where P is the number of positive OAM modes used in the training phase. For generating the $\ell_{\bar{p}}$-th mode training signal, the antenna elements in the q-th SBS UCA are excited with the signal s_q and with successive phase shifts $\varphi_m^q=\ell_{\bar{p}}\phi_m^q=2\pi(m-1)\ell_{\bar{p}}/M, m=1,2,\ldots,M$, so that the phase has an increment of $2\pi\ell_{\bar{p}}$ after a full turn. For an arbitrary point $A(r,\theta,\varphi)$ in the far field, the electric field intensity $E_q(\mathbf{r},\ell_{\bar{p}})$ generated by the q-th SBS is given by [13], [25]

$$\begin{aligned}
&E_q(\mathbf{r},\ell_{\bar{p}})=\\
&-j\frac{\mu_0\omega}{4\pi}\sum_{m=1}^{M}e^{i\ell_{\bar{p}}\phi_m^q}\int|\mathbf{r}-\bar{\mathbf{r}}_m^q|^{-1}e^{ik|\mathbf{r}-\bar{\mathbf{r}}_m^q|}d\overline{V}_m^q\cdot s_q\\
&\approx-j\frac{\mu_0\omega d}{4\pi}\frac{e^{ikr}}{r}\sum_{m=1}^{M}e^{-i(\mathbf{k}\cdot\bar{\mathbf{r}}_m^q-\ell_{\bar{p}}\phi_m^q)}\cdot s_q\\
&\approx-j\frac{\mu_0\omega dMe^{ikr}e^{i\ell_{\bar{p}}\varphi}}{4\pi r}i^{-\ell_{\bar{p}}}J_{\ell_{\bar{p}}}(kR_r\sin\theta)\cdot s_q,
\end{aligned}\tag{1}$$

where $\mathbf{r}$ is the position vector of the point $A(r,\theta,\varphi)$ in $\mathrm{Z}_q^S-\mathrm{X}_q^S\mathrm{O}_q^S\mathrm{Y}_q^S$, i is the imaginary unit, j is the constant current density of the dipole, d is the electric dipole length, μ_0 is the magnetic permeability in a classical vacuum, $\omega=2\pi f$ is the circular frequency, $\mathbf{k}$ is the wave vector and $k=|\mathbf{k}|=2\pi f/c$ is the wave number corresponding to subcarrier frequency f, c is the speed of light in a classical vacuum, $J_{\ell_{\bar{p}}}(\cdot)$ is the $\ell_{\bar{p}}$th-order Bessel function of the first kind, R_r is the radius of the SBS UCAs, $\bar{\mathbf{r}}_m^q=R_r\left(\mathbf{x}_q^S\cos\phi_m^q+\mathbf{y}_q^S\sin\phi_m^q\right)$, $\mathbf{x}_q^S$ and $\mathbf{y}_q^S$ are the unit vectors of X_q^S-axis and Y_q^S-axis.

Then, the received signals of N elements in the MBS UCA are combined, which can be formulated in $\mathrm{Z}_M-\mathrm{X}_M\mathrm{O}_M\mathrm{Y}_M$ as (2) [9], where $\mathbf{r}_q$ is the position vector of the point

$$\begin{aligned}
E(\ell_{\bar{p}})&=\sum_{n=1}^{N}\sum_{q=1}^{Q}E_q(\mathbf{r}_q,\ell_{\bar{p}})+z(\ell_{\bar{p}})\\
&=-j\frac{\mu_0\omega}{4\pi}\sum_{n=1}^{N}\sum_{q=1}^{Q}\sum_{m=1}^{M}e^{i\ell_{\bar{p}}\phi_m^q}\int|\mathbf{r}_q-\bar{\mathbf{r}}_m^q+\bar{\mathbf{r}}_n|^{-1}e^{ik|\mathbf{r}_q-\bar{\mathbf{r}}_m^q+\bar{\mathbf{r}}_n|}d\overline{V}_m^q\cdot s_q+z(\ell_{\bar{p}})\\
&\approx-j\frac{\mu_0\omega d}{4\pi}\sum_{n=1}^{N}e^{i\mathbf{k}\cdot\bar{\mathbf{r}}_n}\cdot\sum_{q=1}^{Q}\frac{e^{ikr_q}}{r_q}\cdot\sum_{m=1}^{M}e^{-i(\mathbf{k}\cdot\bar{\mathbf{r}}_m^q-\ell_{\bar{p}}\phi_m^q)}s_q+z(\ell_{\bar{p}})\\
&\approx-j\frac{\mu_0\omega dMN}{4\pi}i^{-\ell_{\bar{p}}}\sum_{q=1}^{Q}s_q\frac{e^{ikr_q}}{r_q}e^{i\ell_{\bar{p}}\varphi_q}J_{\ell_{\bar{p}}}(kR_r\sin\theta_q)J_0(kR_t\sin\theta_q)+z(\ell_{\bar{p}}),
\end{aligned}\tag{2}$$

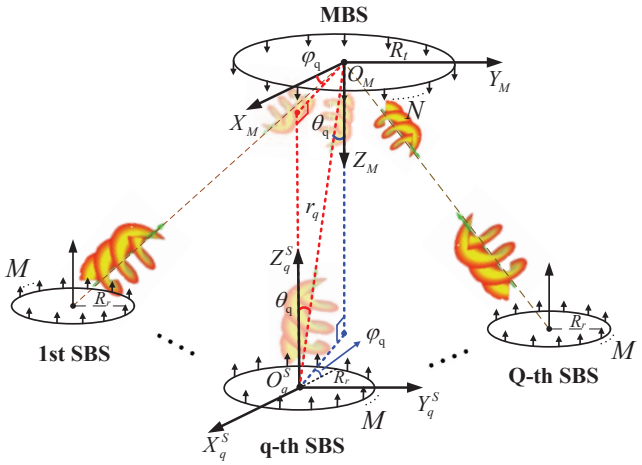

Fig. 2: The geometrical model of the UCA-based MU-OAM system [9].

$\mathrm{O}_q^S(r_q, \theta_q, \varphi_q)$, R_t is the radius of the MBS UCA, $\bar{\mathbf{r}}_n = R_t\left(\mathbf{x}_M \cos\phi_n + \mathbf{y}_M \sin\phi_n\right)$, $\phi_n = 2\pi(n-1)/N$, $\mathbf{x}_M$ and $\mathbf{y}_M$ are the unit vectors of X_M-axis and Y_M-axis, $z(\ell_{\bar{p}})$ is additive white Gaussian noise (AWGN). In practice, the OAM-based training signals from Q SBSs are usually incoherent, i.e.,

$$\mathbb{E}\left\{s_q s_{q'}^*\right\} = \begin{cases} \mathbb{E}\left\{|s_q|^2\right\}, & q = q', \\ 0, & q \neq q'. \end{cases} \tag{3}$$

III. The MU-OAM AoA Estimation Based on Recursive ESPRIT Algorithm

A. Problem Formulation

Neglecting constant terms and performing phase compensation, the training signal in (2) can be simplified as

$$E'(\ell_{\bar{p}}) = \sum_{q=1}^{Q} s_q \frac{e^{ikr_q}}{r_q} e^{i\ell_{\bar{p}}\varphi_q} J_{\ell_{\bar{p}}}(kR_r \sin\theta_q) J_0(kR_t \sin\theta_q) + z'(\ell_{\bar{p}}) \tag{4}$$

where $z'(\ell_{\bar{p}}) = -\frac{4\pi}{j\mu_0\omega dMN} i^{\ell_{\bar{p}}} \cdot z(\ell_{\bar{p}})$ is the related noise. All the received training signals on the $2P+1$ OAM modes can be collected in the vector

$$\mathbf{E}' = \left[E'(-\ell_P), \cdots, E'(0), \cdots, E'(\ell_P)\right]^{\mathrm{T}}. \tag{5}$$

Without loss of generality, the multiplexed modes are assumed to satisfy $\ell_{\bar{p}+1} - \ell_{\bar{p}} = 1$. *The purpose of the MU-OAM AoA estimation is to obtain the elevation and azimuthal angles* $\{(\theta_q, \varphi_q)|q = 1, 2, \cdots, Q\}$ *of all the SBSs from* $\mathbf{E}'$.

B. Estimation of θ_q and φ_q

From (4), we can observe that φ_q and θ_q are both intrinsically related to the OAM mode $\ell_{\bar{p}}$, since φ_q appears in the phase term $e^{i\ell_{\bar{p}}\varphi_q}$ and θ_q in the amplitude term $J_{\ell_{\bar{p}}}(kR_r \sin\theta_q)$ of the training signals. Accordingly, we estimate $\{(\theta_q, \varphi_q)|q = 1, 2, \cdots, Q\}$ by processing $\mathbf{E}'$ in the OAM mode domain. The vector $\mathbf{E}'$ is given in compact form as

$$\mathbf{E}' = \mathbf{A}\tilde{\mathbf{s}} + \mathbf{z}', \tag{6}$$

where the $(2P+1) \times Q$ *direction matrix* takes the form $\mathbf{A} = [\mathbf{a}(\theta_1, \varphi_1), \cdots, \mathbf{a}(\theta_q, \varphi_q), \cdots, \mathbf{a}(\theta_Q, \varphi_Q)]$ and the vector $\mathbf{a}(\theta_q, \varphi_q) = [e^{-i\ell_P\varphi_q} J_{-\ell_P}(kR_r \sin\theta_q), \cdots, J_0(kR_r \sin\theta_q), \cdots, e^{i\ell_P\varphi_q} J_{\ell_P}(kR_r \sin\theta_q)]^{\mathrm{T}}$ contains the AoA information of the q-th SBS, $\tilde{\mathbf{s}} = \mathbf{\Sigma}\mathbf{s}$, $\mathbf{\Sigma} = \mathrm{diag}\{J_0(kR_t \sin\theta_1)e^{ikr_1}/r_1, \cdots, J_0(kR_t \sin\theta_Q)e^{ikr_Q}/r_Q\}$, $\mathbf{s} = [s_1, \cdots, s_Q]^{\mathrm{T}}$, and $\mathbf{z}'$ is the noise vector.

By introducing the $(2P-1) \times (2P+1)$ matrices $\Delta^{(-1)} = [\mathbf{I}_{2P-1}, \mathbf{0}_{(2P-1)\times 2}]$, $\Delta^{(0)} = [\mathbf{0}_{(2P-1)\times 1}, \mathbf{I}_{2P-1}, \mathbf{0}_{(2P-1)\times 1}]$ and $\Delta^{(1)} = [\mathbf{0}_{(2P-1)\times 2}, \mathbf{I}_{2P-1}]$ that select the first, middle, and last $2P-1$ rows of $\mathbf{a}(\theta_q, \varphi_q)$, we can choose a subset of the elements of $\mathbf{a}(\theta_q, \varphi_q)$ to obtain the the three vectors

$$\mathbf{a}_q^{(\gamma)} = \Delta^{(\gamma)}\mathbf{a}(\theta_q, \varphi_q), \quad \gamma = -1, 0, 1, \tag{7}$$

such that the phases (excluding the Bessel functions) of $\mathbf{a}_q^{(0)}$, $e^{i\varphi_q}\mathbf{a}_q^{(-1)}$ and $e^{-i\varphi_q}\mathbf{a}_q^{(1)}$ are the same. Moreover, considering the recursive relation, the characteristic of Bessel functions,

$$J_{x-1}(\xi) + J_{x+1}(\xi) = \frac{2x}{\xi} J_x(\xi) \tag{8}$$

the three vectors $\mathbf{a}_q^{(-1)}$, $\mathbf{a}_q^{(0)}$ and $\mathbf{a}_q^{(1)}$ satisfy the relationship

$$\mathbf{\Gamma}\mathbf{a}_q^{(0)} = \mu_q \mathbf{a}_q^{(-1)} + \mu_q^* \mathbf{a}_q^{(1)}, \tag{9}$$

where $\mu_q = \sin\theta_q e^{i\varphi_q}$, and $\mathbf{\Gamma} = (2/(kR_r))\mathrm{diag}\{-(\ell_P - 1), \cdots, \ell_P - 1\}$. Correspondingly, applying the equivalence (9) to all the columns of the direction matrix $\mathbf{A}$ yields

$$\mathbf{\Gamma}\mathbf{A}^{(0)} = \mathbf{A}^{(-1)}\mathbf{\Phi} + \mathbf{A}^{(1)}\mathbf{\Phi}^{\mathrm{H}}, \tag{10}$$

where $\mathbf{A}^{(\gamma)} = \Delta^{(\gamma)}\mathbf{A}, \gamma = -1, 0, 1$, $\mathbf{\Phi} = \mathrm{diag}\{\mu_1, \cdots, \mu_Q\}$.

The covariance matrix of $\mathbf{E}'$ can be represented as

$$\mathbf{R}_{\mathbf{E}'} = \mathbb{E}\left\{\mathbf{E}'\mathbf{E}'^{\mathrm{H}}\right\} = \mathbf{A}\mathbf{R}_{\tilde{\mathbf{s}}}\mathbf{A}^{\mathrm{H}} + \mathbf{R}_{\mathbf{z}'}, \tag{11}$$

where $\mathbf{R}_{\tilde{\mathbf{s}}} = \mathbf{\Sigma}\mathbb{E}\left\{\mathbf{s}\mathbf{s}^{\mathrm{H}}\right\}\mathbf{\Sigma}^{\mathrm{H}}$, $\mathbf{R}_{\mathbf{z}'} = \mathbb{E}\left\{\mathbf{z}'\mathbf{z}'^{\mathrm{H}}\right\}$. Then, the eigenvalue decomposition (EVD) of $\mathbf{R}_{\mathbf{E}'}$ is written as

$$\mathbf{R}_{\mathbf{E}'} = \sum_{\bar{p}=1}^{2P+1} \lambda_{\bar{p}} \mathbf{u}_{\bar{p}} \mathbf{u}_{\bar{p}}^{\mathrm{H}} = \mathbf{U}\mathbf{\Lambda}\mathbf{U}^{\mathrm{H}}, \tag{12}$$

where $\{\lambda_{\bar{p}}|\bar{p} = 1, 2, \cdots, 2P+1\}$ are the eigenvalues of $\mathbf{R}_{\mathbf{E}'}$, $\mathbf{\Lambda} = \mathrm{diag}\{\lambda_1, \lambda_2, \cdots, \lambda_{2P+1}\}$, $\mathbf{u}_{\bar{p}}$ is the eigenvector corresponding to the eigenvalue $\lambda_{\bar{p}}$, $\mathbf{U} = [\mathbf{u}_1, \cdots, \mathbf{u}_{2P+1}]$. In practice, the training signal and noise are independent of each other, thus, the covariance matrix $\mathbf{R}_{\mathbf{E}'}$ can be decomposed into two mutually orthogonal parts:

$$\mathbf{R}_{\mathbf{E}'} = \mathbf{U}_s\mathbf{\Lambda}_s\mathbf{U}_s^{\mathrm{H}} + \mathbf{U}_n\mathbf{\Lambda}_n\mathbf{U}_n^{\mathrm{H}}, \tag{13}$$

where $\mathbf{\Lambda}_s$ is the Q-dimensional diagonal matrix that contains the Q largest eigenvalues of $\mathbf{R}_{\mathbf{E}'}$, $\mathbf{U}_s$ is the $(2P+1) \times Q$ signal subspace spanned by the eigenvectors corresponding to the Q larger eigenvalues, $\mathbf{\Lambda}_n$ is the $(2P-Q+1)$-dimensional diagonal matrix that contains the $2P-Q+1$ smaller eigenvalues of $\mathbf{R}_{\mathbf{E}'}$, $\mathbf{U}_n$ is the $(2P+1) \times (2P-Q+1)$ noise subspace spanned by the eigenvectors corresponding to the $2P-Q+1$ smaller eigenvalues.

Since the range of $\mathbf{U}_s$ is equal to that of $\mathbf{A}$, i.e., $\mathcal{R}\{\mathbf{U}_s\} = \mathcal{R}\{\mathbf{A}\}$, there exists a nonsingular matrix $\mathbf{T}$ such that

$$\mathbf{U}_s = \mathbf{A}\mathbf{T}. \tag{14}$$

Algorithm 1 AoA Estimation by Recursive ESPRIT

Input: $\mathbf{E}'$
Output: $\{(\hat{\theta}_q, \hat{\varphi}_q)|q = 1, 2, \cdots, Q\}$
procedure
$\mathbf{R}_{\mathbf{E}'} \leftarrow \mathbf{R}_{\mathbf{E}'} = \mathbb{E}\left\{\mathbf{E}'\mathbf{E}'^{\mathrm{H}}\right\}$
$\mathbf{U}$, $\mathbf{\Lambda} \leftarrow$ decompose $\mathbf{R}_{\mathbf{E}'}$ such that $\mathbf{U}\mathbf{\Lambda}\mathbf{U}^{\mathrm{H}}$
$\mathbf{\Lambda} \leftarrow \mathrm{diag}\{\lambda_1, \cdots, \lambda_{2P+1}\}$, $\lambda_1 \geq \cdots \geq \lambda_{2P+1}$
$\mathbf{\Lambda}_s \leftarrow \mathrm{diag}\{\lambda_1, \cdots, \lambda_Q\}$
$\mathbf{U}_s \leftarrow$ the Q columns of $\mathbf{U}$ corresponding to $\mathbf{\Lambda}_s$
$\mathbf{U}_s^{(\gamma)} \leftarrow \Delta^{(\gamma)}\mathbf{U}_s, \gamma = -1, 0, 1$
$\mathbf{\Gamma} \leftarrow (2/(kR_r)) \cdot \mathrm{diag}\{-(\ell_P - 1), \cdots, \ell_P - 1\}$
$\widehat{\mathbf{\Psi}} \leftarrow \left[\mathbf{U}_s^{(-1)}, \mathbf{U}_s^{(1)}\right]^{\dagger} \mathbf{\Gamma}\mathbf{U}_s^{(0)}$
$\mathbf{\Psi} \leftarrow$ the first Q rows of $\widehat{\mathbf{\Psi}}$
$\mathbf{\Psi}' \leftarrow$ the last Q rows of $\widehat{\mathbf{\Psi}}$
$\mathbf{\Phi} \leftarrow$ decompose $\mathbf{\Psi}$ such that $\mathbf{T}\mathbf{\Phi}\mathbf{T}^{-1}$
$\mathbf{\Phi}^{\mathrm{H}} \leftarrow$ decompose $\mathbf{\Psi}'$ such that $\mathbf{T}\mathbf{\Phi}^{\mathrm{H}}\mathbf{T}^{-1}$
for $q = 1 \rightarrow Q$ **do**
    $\hat{\varphi}_q^0 \leftarrow \arg\left(\mathbf{\Phi}(q, q)\right)$
    $\hat{\varphi}_q^1 \leftarrow -\arg\left(\mathbf{\Phi}^{\mathrm{H}}(q, q)\right)$
    $\hat{\varphi}_q \leftarrow (\hat{\varphi}_q^0 + \hat{\varphi}_q^1)/2$
    $\hat{\theta}_q^0 \leftarrow \arcsin\left(|\mathbf{\Phi}(q, q)|\right)$
    $\hat{\theta}_q^1 \leftarrow \arcsin\left(|\mathbf{\Phi}^{\mathrm{H}}(q, q)|\right)$
    $\hat{\theta}_q \leftarrow (\hat{\theta}_q^0 + \hat{\theta}_q^1)/2$
end for
end procedure

Therefore, the signal subspace $\mathbf{U}_s$ can be similarly denoted as

$$\begin{aligned}\mathbf{\Gamma}\mathbf{U}_s^{(0)} &= \mathbf{\Gamma}\mathbf{A}^{(0)}\mathbf{T} \\ &= \mathbf{A}^{(-1)}\mathbf{T}\mathbf{T}^{-1}\mathbf{\Phi}\mathbf{T} + \mathbf{A}^{(1)}\mathbf{T}\mathbf{T}^{-1}\mathbf{\Phi}^{\mathrm{H}}\mathbf{T} \\ &= \mathbf{U}_s^{(-1)}\mathbf{\Psi} + \mathbf{U}_s^{(1)}\mathbf{\Psi}', \end{aligned} \tag{15}$$

where $\mathbf{U}_s^{(\gamma)} = \Delta^{(\gamma)}\mathbf{U}_s, \gamma = -1, 0, 1$, $\mathbf{\Psi} = \mathbf{T}^{-1}\mathbf{\Phi}\mathbf{T}$ and $\mathbf{\Psi}' = \mathbf{T}^{-1}\mathbf{\Phi}^{\mathrm{H}}\mathbf{T}$. Based on the (15), one obtains

$$\begin{bmatrix} \mathbf{\Psi} \\ \mathbf{\Psi}' \end{bmatrix} = \left[\mathbf{U}_s^{(-1)}, \mathbf{U}_s^{(1)}\right]^{\dagger} \mathbf{\Gamma}\mathbf{U}_s^{(0)}, \tag{16}$$

and the eigenvalues of $\mathbf{\Psi}$ and $\mathbf{\Psi}'$ give the diagonal elements of $\mathbf{\Phi}$ and $\mathbf{\Phi}^{\mathrm{H}}$, which are $\{\mu_q = \sin\theta_q e^{i\varphi_q} | q = 1, 2, \cdots, Q\}$ and $\{\mu_q^* = \sin\theta_q e^{-i\varphi_q} | q = 1, 2, \cdots, Q\}$ respectively. The eigenvalues of $\mathbf{\Psi}$ and $\mathbf{\Psi}'$ therefore yield automatically paired azimuth angle φ_q and elevation angle θ_q, and the detailed procedure of the proposed recursive ESPRIT algorithm is shown in Algorithm 1. The computational complexity of the core steps is summarized in Table 1, and the total complexity of proposed algorithm mainly originates from the EVDs and Moore-Penrose pseudo-inverse.

Unlike the FFT-based AoA estimation method in [9], the proposed recursive ESPRIT algorithm can directly obtain the closed-form solution of azimuth and elevation angles only by signal processing in the OAM mode domain, without 2-D spectral searching in the frequency and OAM mode domains and matching independently estimated elevation and azimuth angles, which thus saves the training overhead. Therefore, the SE of the MU-OAM system would be further improved by using the proposed recursive ESPRIT method. Moreover, the total complexity of the proposed recursive ESPRIT algorithm is compared with that of the FFT-based estimation method in Fig.3, where the FFT-based estimation method is assumed to utilize $W = 32$ subcarriers for AoA estimation. Due to the EVDs and Moore-Penrose pseudo-inverse in the algorithm process, the complexity of the proposed recursive ESPRIT algorithm is higher than that of FFT-based estimation method when P and Q are large.

TABLE I: The complexity of the recursive ESPRIT algorithm.

Step	Complexity	Total Complexity
Step 2	$\mathcal{O}\left(P^2\right)$	
Step 3	$\mathcal{O}\left(P^3\right)$	
Step 9	$\mathcal{O}\left(QP^2\right)$	$\mathcal{O}\left(P^3 + QP^2 + Q^3\right)$
Step 12	$\mathcal{O}\left(Q^3\right)$	
Step 13	$\mathcal{O}\left(Q^3\right)$	

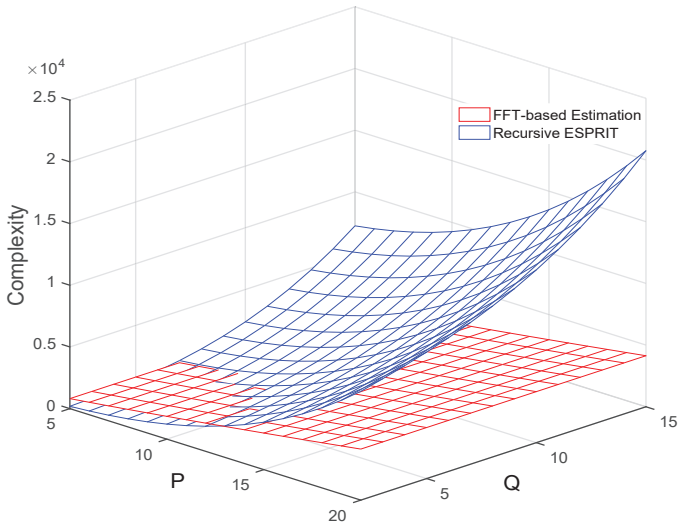

Fig. 3: The complexities of the recursive ESPRIT algorithm and the FFT-based estimation method in [9] vs. P and Q with $W = 32$.

IV. Simulation Results

In this part, we first verify the proposed recursive ESPRIT algorithm at different SNRs by numerical simulations. Thereafter, we compare the estimation error of the recursive ESPRIT algorithm with that of the FFT-based estimation method in [9]. At last, the SE of the MU-OAM system with transmitting preprocessing (TP) [9] based on the estimated AoA is compared with that without TP. In the simulations we choose the subcarrier frequency $f = 8.976$GHz corresponding to the wave number $k = 188$ for the proposed recursive ESPRIT algorithm, and $W = 32$ subcarriers from 8.212GHz to 9.692GHz corresponding to the wave numbers $k_1, k_2, \cdots, k_{32} = 172, 181, \cdots, 203$ for the FFT-based AoA estimation method in [9], $M = 12$, $Q = 3$, $N = 36$, $P = 5$ with OAM modes $\ell_1, \ell_2, \cdots, \ell_{11} = -5, -4, \cdots, +5$, $R_t = 30\lambda$, $R_r = 15\lambda$, $\lambda = 2\pi/k$, $(\theta_1, \varphi_1) = (10°, 20°)$, $(\theta_2, \varphi_2) = (15°, 45°)$, $(\theta_3, \varphi_3) = (30°, 60°)$. It is noteworthy

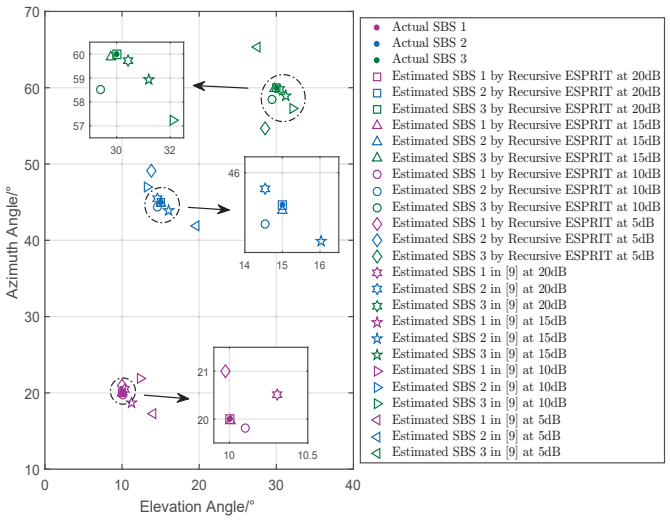

Fig. 4: The MU-OAM AoA estimation results with $P = 5$ and $W = 1$ for the recursive ESPRIT algorithm and $P = 5$ and $W = 32$ for the FFT-based method in [9].

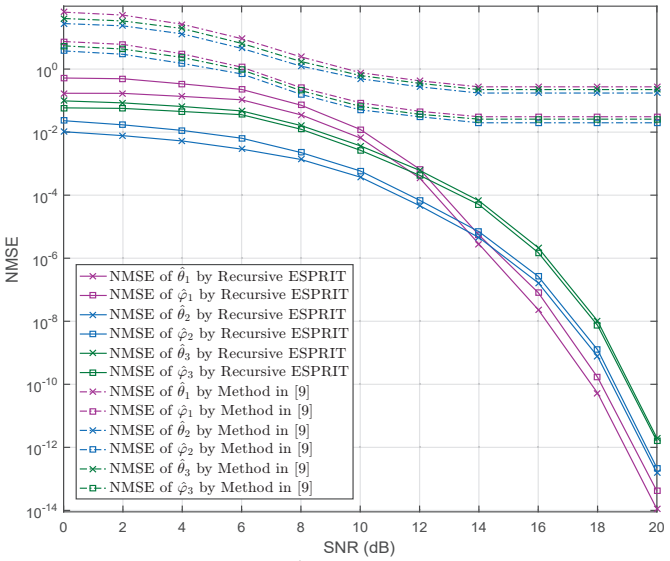

Fig. 5: The NMSEs of $\{(\hat{\theta}_q, \hat{\varphi}_q)|q = 1, 2, 3\}$ vs. SNR with $P = 5$ and $W = 1$ for the recursive ESPRIT algorithm and $P = 5$ and $W = 32$ for the FFT-based method in [9].

that the SNRs refer to the ratio of the received signal power to the noise power in all the figures.

Fig.4 shows an intuitive example, from which the accuracy of the proposed recursive ESPRIT algorithm is visually compared the results of the FFT-based estimation method in [9]. It can be concluded that with the increase of SNR, the estimated AoAs of Q SBSs obtained by both methods approach the actual values. Meanwhile, under the same SNR, the estimated AoAs obtained by the recursive ESPRIT algorithm are closer to the actual value than those obtained by the estimation method in [9].

The normalized mean-squared errors (NMSEs) of $\{(\hat{\theta}_q, \hat{\varphi}_q)|q = 1, 2, 3\}$ obtained by recursive ESPRIT algorithm and the FFT-based method in [9] are plotted in Fig.5. The NMSE is defined as $\mathbb{E}\{(\hat{a} - a)^2/a^2\}$, where $\hat{a}$ is the estimate of a. The NMSEs of $\{(\hat{\theta}_q, \hat{\varphi}_q)|q = 1, 2, 3\}$ obtained by the recursive

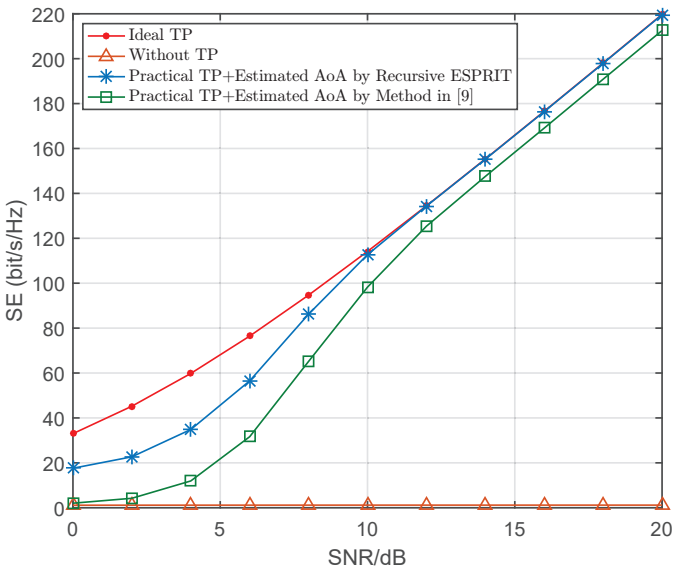

Fig. 6: The SE of the MU-OAM system. TP: transmitting preprocessing.

ESPRIT algorithm are greatly lower than those obtained by the method in [9]. Especially under medium and high SNR, the accuracy advantage of the proposed recursive ESPRIT algorithm is more obvious.

In Fig.6, the SE of the MU-OAM system with TP assisted by the estimated AoAs is compared with the SEs of a system without TP and of a system with ideal TP, which employs the actual AoAs of Q SBSs. The SE of the MU-OAM system is significantly improved after applying TP with the estimated AoAs, so that it is close to the SE of the ideal system. It follows that reliable AoA estimation is necessary in MU-OAM systems. More importantly, in contrast to the FFT-based estimation method [9], the proposed recursive ESPRIT algorithm only uses a single subcarrier for the AoA estimation, greatly reducing the training overhead and thus achieving higher SE.

V. Conclusions

To further improve the SE of the MU-OAM system, we propose a novel recursive ESPRIT algorithm, which can accurately and reliably estimate the azimuth and elevation angles of multiple SBSs based on the recursive characteristic of the Bessel function in OAM training signals. Compared with the existing FFT-based MU-OAM AoA estimation method [9], the proposed method has higher accuracy with less training overhead, which is more efficient. With the aid of the proposed method, the SE of the MU-OAM system is significantly improved, approaching the SE of the ideal system.

References

[1] Z. Zhang, Y. Xiao, Z. Ma, M. Xiao, and et al., "6G wireless networks: Vision, requirements, architecture, and key technologies," *IEEE Veh. Technol. Mag.*, vol. 14, no. 3, pp. 28–41, Sept. 2019.

[2] W.-X. Long, R. Chen, M. Moretti, W. Zhang, and J. Li, "A promising technology for 6G wireless networks: Intelligent reflecting surface," *J. Commun. Inf. Networks*, vol. 6, no. 1, pp. 1–16, Mar. 2021.

[3] (2018, Sept.) World radiocommunication conference (WRC). [Online]. Available: https://www.itu.int/en/ITU-R/conferences/wrc/Pages/default.aspx.

[4] E. Hossain, M. Rasti, H. Tabassum, and A. Abdelnasser, "Evolution toward 5G multi-tier cellular wireless networks: An interference management perspective," *IEEE Wireless Commun.*, vol. 21, no. 3, pp. 118–127, Jun. 2014.

[5] E. Garro, C. Barjau, D. Gomez-Barquero, J. Kim, S. I. Park, and N. Hur, "Layered division multiplexing with co-located multiple-input multiple-output schemes," *IEEE Trans. Broadcast.*, vol. 66, no. 1, pp. 9–20, Mar. 2020.

[6] J. Xiong, Y. Fang, P. Cheng, Z. Shi, and W. Zhang, "Distributed caching in converged networks: A deep reinforcement learning approach," *IEEE Trans. Broadcast.*, vol. 67, no. 1, pp. 201–211, Mar. 2021.

[7] U. Siddique, H. Tabassum, E. Hossain, and D. I. Kim, "Wireless backhauling of 5G small cells: Challenges and solution approaches," *IEEE Wireless Commun.*, vol. 22, no. 5, pp. 22–31, Oct. 2015.

[8] N. Wang, E. Hossain, and V. K. Bhargava, "Backhauling 5G small cells: A radio resource management perspective," *IEEE Wireless Commun.*, vol. 22, no. 5, pp. 41–49, Oct. 2015.

[9] W.-X. Long, R. Chen, M. Moretti, J. Xiong, and J. Li, "Joint spatial division and coaxial multiplexing for downlink multi-user OAM wireless backhaul," *IEEE Trans. Broadcast.*, vol. 67, no. 4, pp. 879–893, Dec. 2021.

[10] L. Allen, M. Beijersbergen, R. Spreeuw, and J. Woerdman, "Orbital angular momentum of light and the transformation of laguerre-gaussian laser modes," *Physical Review A*, vol. 45, no. 11, p. 8185, 1992.

[11] W. Zhang, S. Zheng, X. Hui, R. Dong, X. Jin, H. Chi, and X. Zhang, "Mode division multiplexing communication using microwave orbital angular momentum: An experimental study," *IEEE Trans. Wireless Commun.*, vol. 16, no. 2, pp. 1308–1318, Feb. 2017.

[12] C. Zhang and Y. Zhao, "Orbital angular momentum nondegenerate index mapping for long distance transmission," *IEEE Trans. Wireless Commun.*, vol. 18, no. 11, pp. 5027–5036, Nov. 2019.

[13] R. Chen, W. Long, X. Wang, and J. Li, "Multi-mode OAM radio waves: generation, angle of arrival estimation and reception with UCAs," *IEEE Trans. Wireless Commun.*, vol. 19, no. 10, pp. 6932–6947, Oct. 2020.

[14] R. Chen, H. Zhou, M. Moretti, X. Wang, and J. Li, "Orbital angular momentum waves: Generation, detection, and emerging applications," *IEEE Commun. Surveys Tuts.*, vol. 22, no. 2, pp. 840–868, 2nd Quart. 2020.

[15] T. Hu, Y. Wang, X. Liao, and J. Zhang, "OAM-based beam selection for indoor millimeter wave MU-MIMO systems," *IEEE Commun. Lett.*, vol. 25, no. 5, pp. 1702–1706, 2021.

[16] H. Tian, Z. Liu, W. Xi, G. Nie, L. Liu, and H. Jiang, "Beam axis detection and alignment for uniform circular array-based orbital angular momentum wireless communication," *IET Commun.*, vol. 10, no. 1, pp. 44–49, Jan. 2016.

[17] V. Vahidiniai, M. Atashbar, and S. Hosseinzadeh, "Array misalignment angle value estimation for OAM-based communication system," *J. of the Franklin Inst.*, vol. 358, no. 18, pp. 10 213–10 231, Dec. 2021.

[18] D. Chen, B. Chen, and G. Qin, "Angle estimation using ESPRIT in MIMO radar," *Electron. Lett.*, vol. 44, no. 12, pp. 770–771, Jun. 2008.

[19] X. Zhang, L. Xu, L. Xu, and D. Xu, "Direction of departure (DoD) and direction of arrival (DoA) estimation in MIMO radar with reduced-dimension MUSIC," *IEEE Commun. Lett*, vol. 14, no. 12, pp. 1161–1163, Dec. 2010.

[20] X. P. Wang, L. Y. Wang, X. M. Li, and G. Bi, "Nuclear norm minimization framework for DOA estimation in MIMO radar," *Signal Processing*, vol. 135, pp. 147–152, 2017.

[21] R. Roy and T. Kailath, "ESPRIT-estimation of signal parameters via rotational invariance techniques," *IEEE Trans. Acoust., Speech, Signal Processing*, vol. 37, no. 7, pp. 984–995, Jul. 1989.

[22] K. Liu, Y. Cheng, X. Li, Y. Qin, H. Wang, and Y. Jiang, "Generation of orbital angular momentum beams for electromagnetic vortex imaging," *IEEE Antennas Wireless Propag. Lett.*, vol. 15, pp. 1873–1876, Mar. 2016.

[23] R. Chen, W. Yang, H. Xu, and J. Li, "A 2-D FFT-based transceiver architecture for OAM-OFDM systems with UCA antennas," *IEEE Trans. Veh. Technol.*, vol. 67, no. 6, pp. 5481–5485, Jun. 2018.

[24] R. Chen, H. Xu, M. Moretti, and J. Li, "Beam steering for the misalignment in UCA-based OAM communication systems," *IEEE Wireless Commun. Lett.*, vol. 7, no. 4, pp. 582–585, Aug. 2018.

[25] W.-X. Long, R. Chen, M. Moretti, and J. Li, "AoA estimation for OAM communication systems with mode-frequency multi-time ESPRIT method," *IEEE Trans. Veh. Technol.*, vol. 70, no. 5, pp. 5094–5098, May 2021.